# Parametric Homogenized Model for Inclusion of Eddy Currents and Hysteresis in 2-D Finite-Element Simulation of Electrical Machines

Christian Krüttgen, Simon Steentjes, Gregor Glehn, and Kay Hameyer

Institute of Electrical Machines, RWTH Aachen University, NRW 52062 Aachen, Germany

**Consideration of a fully coupled lamination model with eddy currents and magnetic hysteresis in standard finite-element (FE) models is prohibitively expensive in terms of implementation effort, memory requirements, and computation time. Instead, this paper utilizes an algebraic approximation of the lamination model as a conventional constitutive relationship in (2-D) FE simulations of electrical machines. The TEAM problem 32, that is a test case for validating 2-D magnetic field analysis codes, which account for magnetic hysteresis, serves as a validation example. Extraction of the parameters of the parametric model and comparison with results using the fully coupled lamination model are presented. This pragmatic approach turns out to be quite accurate and efficient.**

*Index Terms*— **Eddy currents, electrical machines, homogenization, magnetic hysteresis, system identification.**

## I. Introduction

SOFT MAGNETIC cores of rotating electrical machines are laminated for the reduction of eddy current losses and exhibit magnetic hysteresis when subjected to a time-varying magnetic-field strength. These closely intertwined phenomena alter the overall behavior and performance of the electrical machine, that is, iron losses and magnetizability. Accounting for these is a critical problem to the accurate electrical machine design. A fine discretization of each single lamination and application of a dynamic hysteresis model [1]–[3] as a constitutive relationship in standard finite-element (FE) models is prohibitively expensive in terms of implementation effort, memory requirements, and computation time. The heterogeneous multiscale method (HMM) enables connecting the lamination model (mesoscale) with the macroscopic model of the electrical machine. However, a monolithic implementation of the HMM, such as in [4], leads to models one or two orders of magnitude larger than the initial non-homogenized model, not to mention the significant implementation work. Instead of this, in this paper, the method proposed in [5] that separates the HMM approach into two independent steps is incorporated in 2-D FE simulation so as to deliver the vectorial macroscopic constitutive relationship accounting for the intricate coupling of magnetic hysteresis and eddy currents at the lamination level. The TEAM problem 32 that is a test case for validating 2-D magnetic-field analysis codes with hysteresis serves as a validation example.

## II. Lamination Model and Algebraic Approximation

The quantitative description of the magnetization process in a thin long sheet (width $w$, length $l$, and thickness $d$, respectively, directed along the $x$-, $y$-, and $z$-axis) when neglecting edge effects is reduced to the integration of a (1-D) penetration equation that links the magnitudes of the magnetic field $\mathbf{h}$, the magnetic flux density $\mathbf{b}$, and the electric-field strength $\mathbf{e}$ within a material with specific electrical conductivity $\sigma_\mathrm{e}$ and a non-linear, hysteretic relation $\mathbf{b}(\mathbf{h}, \mathrm{history}, \dots)$. This can be written as

$$\frac{\partial^2 \mathbf{h}(z,t)}{\partial z^2} = \sigma_e \frac{\partial \mathbf{b}(z,t)}{\partial t} \tag{1}$$

where $\mathbf{b}(z,t) = \mathbf{b}(\mathbf{h}(z,t), \mathrm{history}, \dots)$ is given by a vector hysteresis model.

Different methods are available to solve the coupled Maxwell equations with hysteresis (1). Among others, finite-difference schemes, various magnetic equivalent circuits, FE solutions, and the parametric magnetodynamic model exist [3], [6]–[8], which differ in terms of mathematical structure, implementation work, spatial discretization, and accuracy when applied to voltage- and current-driven problems.

A mesh-free model is proposed in [9] and [10] to reduce the number of unknowns and speed-up simulation times in comparison with the FE solution [7], [8]. Using this approach, the magnetic flux density distribution in the lamination depth ($z \in [-d/2, d/2]$) is approximated by using a truncated Fourier cosine series with $N_\mathrm{b}$ terms

$$\mathbf{b}(z,t) = \sum_{n=0}^{N_\mathrm{b}-1} \mathbf{b}_n(t)\, \alpha_n(z) \tag{2}$$

with $\alpha_n(z) = \cos(2n\pi \frac{z}{d})$. Analog to this, the magnetic field can be approximated by

$$\mathbf{h}_{\mathrm{approx.}}(z,t) = \mathbf{h}_s(t) - \sigma_\mathrm{e} d^2 \sum_{n=0}^{N_\mathrm{b}-1} \frac{\partial \mathbf{b}_n}{\partial t}\, \beta_n(z) \tag{3}$$

where $\mathbf{h}_s(t)$ is the magnetic field at the surface of the lamination and functions $\beta_n(z)$ are defined to fulfill $\beta_n(\pm\frac{d}{2}) = 0$ and $\alpha_n(z) = d^2(\partial^2 \beta_n(z))/(\partial z^2)$.

Weakly satisfying the approximation error between $\mathbf{h}_{\mathrm{approx.}}(z,t)$ and the actual magnetic field $\mathbf{h}(z,t) = \mathbf{h}(\mathbf{b}(z,t))$ yields the following equation system for the magnetic field at the surface [10]:

$$\begin{pmatrix} \mathbf{h}_s(t) \\ 0 \\ \vdots \end{pmatrix} = \frac{1}{d} \int_{-\frac{d}{2}}^{\frac{d}{2}} \mathbf{h}(z,t) \begin{pmatrix} \alpha_0(z) \\ \alpha_1(z) \\ \vdots \end{pmatrix} \mathrm{d}z + \sigma_e d^2 \mathbf{C} \frac{\partial}{\partial t} \begin{pmatrix} \mathbf{b}_0(t) \\ \mathbf{b}_1(t) \\ \vdots \end{pmatrix} \tag{4}$$

Manuscript received November 25, 2016; revised January 13, 2017; accepted January 18, 2017. Date of publication January 27, 2017; date of current version May 26, 2017. Corresponding author: S. Steentjes (e-mail: simon.steentjes@iem.rwth-aachen.de).

Color versions of one or more of the figures in this paper are available online at http://ieeexplore.ieee.org.

Digital Object Identifier 10.1109/TMAG.2017.2660460

with the magnetic field $\mathbf{h}(z,t)$ obtained from the static vector hysteresis model and where the elements of the constant matrix $\mathbf{C}$ are determined by integration over the lamination thickness as [10]

$$C_{\mathrm{m,n}} = \frac{1}{d}\int_{-\frac{d}{2}}^{\frac{d}{2}} \alpha_{\mathrm{m}}(z)\beta_{\mathrm{n}}(z)\mathrm{d}z \tag{5}$$

for $m, n \in [0, N_{\mathrm{b}} - 1]$. Equation (4) can now be solved by an implicit Euler method and an iterative Newton–Raphson (NR) method for the current-driven case [$\mathbf{h}_s(t)$ is known] and for the voltage-driven case [the spatial average of the magnetic flux density $\mathbf{B} = \langle \mathbf{b}(z) \rangle = \mathbf{b}_0(t)$ is known]. Capital letters denote fields at the macroscopic scale (averaged over the lamination thickness). This allows one to calculate the material response to arbitrary excitation waveforms.

However, the direct incorporation of the 1-D lamination model into 2-D FE simulations of laminated-core electrical machines is rather technical and requires several times more degrees of freedom than traditional FE formulations. In addition, the hysteretic material properties may cause problems in the convergence of the nonlinear iteration.

For this purpose, the parametric algebraic model (PAM) given in (6) was proposed in [5] to deliver the vectorial macroscopic constitutive relationship $\mathbf{H}_s(\mathbf{B})$ accounting for the intricate coupling of magnetic hysteresis and eddy currents at the lamination level

$$\mathbf{H}(\mathbf{B}, \dot{\mathbf{B}}, p_k) = \left(p_0 + p_1|\mathbf{B}|^{2p_2}\right)\mathbf{B} + p_3\dot{\mathbf{B}} + \frac{p_4\dot{\mathbf{B}}}{\sqrt{p_5^2 + |\dot{\mathbf{B}}|^2}}. \tag{6}$$

In the following text, both models are validated against the measured data of a non-oriented electrical steel sheet classified as M400-50A. This material was characterized in an Epstein frame under quasistatic, sinusoidal, and arbitrary magnetic flux density waveforms [11]. The static vector hysteresis model constituting the rate-independent material behavior in (4) is parameterized using the measured quasistatic major loop at 1.5 T [11]. Complemented by the measured specific conductivity $\sigma_{\mathrm{e}}$ and the thickness $d$ of the sheet, the mesh-free model (4) is able to simulate the material behavior under arbitrary loads. For validation purposes, the measured magnetic field at the surface of the sheet $H_s = h_s$ is used as model input and the simulated magnetic flux density averaged over the lamination thickness is compared with the measured one. In addition, the parameter of the PAM model is identified in order to minimize the least square approximation error [1], [2]. Fig. 1 shows a comparison of the measured and simulated major hysteresis loops using the PAM and the mesh-free model for time-varying sinusoidal magnetic flux densities of 1 and 1.5 T amplitude at 400-Hz excitation frequency.

It is apparent that the model structure (6) is capable of predicting hysteresis loop shapes with sufficient accuracy and is well-suited to serve as a region-dependent constitutive material model in combination with a reparametrization scheme in the simulation of electrical machines.

## III. Finite-Element Simulation

### A. 2-D Magnetic Vector Potential A-Formulation

A 2-D magnetic-field problem in space domain $\Omega$ with boundary $\Gamma$ and time domain $[0, T]$ is considered.

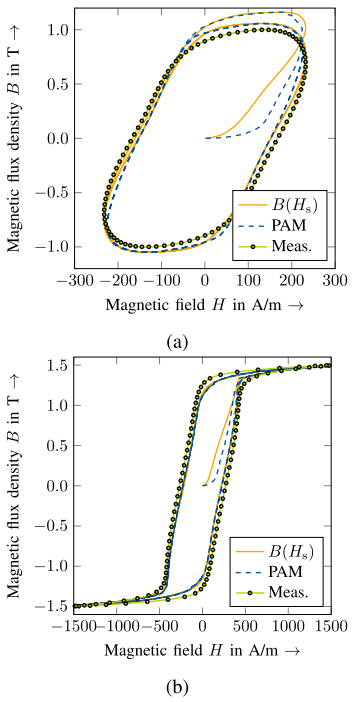


Fig. 1. Comparison of measured data (dots), the mesh-free model (continuous lines), and the parametric approximation (dashed lines) for 400 Hz at (a) 1 and (b) 1.5 T.

The definition of a continuous magnetic vector potential $\mathbf{A}(t)$ by $\nabla \times \mathbf{A}(t) = \mathbf{B}(t)$ ensures $\nabla \cdot \mathbf{B} = 0$. The magnetic vector potential is discretized with the piecewise linear nodal shape functions $w$

$$\mathbf{A}(x, y, t) = \sum_{j=1}^{N_e} a_j(t) \cdot w_j(x, y). \tag{7}$$

Applying a weighted residual approach on Ampere's law yields the weak formulation

$$\int_{\Omega} \mathbf{H} \cdot (\nabla \times w_i) d\Omega + \oint_{\partial\Omega} \mathbf{H} \times w_i d\Gamma = \int_{\Omega_s} \mathbf{J}_s \cdot w_i d\Omega. \tag{8}$$

$\mathbf{J}_s$ is the source current in a subspace $\Omega_s$ and $w_i$ are the weight functions. The closed integral on the boundary is equal to zero due to Neumann ($\mathbf{H} \times n = 0$ on $\Gamma_H$) or Dirichlet ($\mathbf{B} \cdot n = \mathbf{B}_n = 0$ on $\Gamma_B$) boundary conditions with $n$ being the normal vector to the boundary. To solve (8) in the time domain, a time-stepping technique is applied, due to the time dependencies of the hysteretic materials. If $\mathbf{A}(t_n)$ is a given state of the magnetic problem, the state of the next time instant $t_{n+1} = t_n + \Delta t$ is calculated by an iterative NR method. For each NR iteration ($\mathbf{A}^k = \mathbf{A}^{k-1} + \Delta\mathbf{A}^k$), the increment $\Delta\mathbf{A}^k$ has to be calculated. Therefore, (8) is linearized around $\mathbf{A}^{k-1}$. This linearization is obtained by the derivation of (8) with respect to $a_j$, which can be achieved through the differential reluctivity $\mathrm{d}\mathbf{H}/\mathrm{d}a_j = \mathrm{d}\mathbf{H}/\mathrm{d}\mathbf{B} \cdot \nabla \times w_j = \nu_d \cdot \nabla \times w_j$ [12]:

$$\sum_{j=1}^{N_e} \Delta a_j^k \int_{\Omega} (\nu_d \cdot \nabla \times w_j) \cdot (\nabla \times w_i) d\Omega = \int_{\Omega_s} \mathbf{J}_s(t_{n+1}) \cdot w_i \, d\Omega - \int_{\Omega} \mathbf{H}^{k-1} \cdot (\nabla \times w_i) \, d\Omega. \tag{9}$$

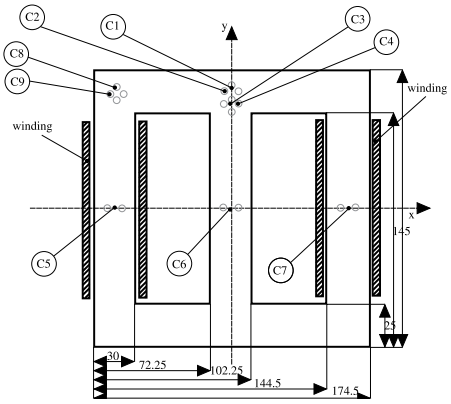


Fig. 2. Geometry of TEAM problem 32 with the excitation coils and the measuring coils.

In the discrete time-stepping scheme, the differential reluctivity can be expressed by

$$\nu_d = \frac{\mathrm{d}\mathbf{H}}{\mathrm{d}\mathbf{B}} = \frac{\Delta\mathbf{H}}{\Delta\mathbf{B}} = \frac{\Delta\mathbf{H}\cdot\Delta\mathbf{B}}{\Delta\mathbf{B}\cdot\Delta\mathbf{B}} \tag{10}$$

with $\Delta\mathbf{H} = \mathbf{H}^{k-1}(t_{n+1}) - \mathbf{H}(t_n)$ and $\Delta\mathbf{B} = \mathbf{B}^{k-1}(t_{n+1}) - \mathbf{B}(t_n)$.

### *B. Solving Process*

To solve the field problem in time domain, the following simulation scheme is applied.

1) *Initialization:* All necessary parameters for the FE formulation as well as material models are set.
2) *Time-Stepping Loop:* The outer loop consists of the time-stepping scheme. For each step, an NR loop is performed to obtain the solution of the next time instant $\mathbf{A}(t_{n+1})$. In the next step, this solution is stored in the hysteretic material models for the previous time step solution.
3) *NR Loop:* For each time step, the NR method is applied to solve the field problem. The initial values are set to $\mathbf{A}^0(t_{n+1}) = \mathbf{A}(t_n)$, $\mathbf{H}^0(t_{n+1}) = \mathbf{H}(t_n)$, and $\nu_d^0(t_{n+1}) = \nu_d(t_n)$. Then, (9) is solved to get $\Delta\mathbf{A}^k$. This yields $\mathbf{A}^k = \mathbf{A}^{k-1} + \Delta\mathbf{A}^k$ and the magnetic flux density $\mathbf{B}^k = \nabla\times\mathbf{A}^k$. With the new magnetic flux density, the magnetic field strength $\mathbf{H}^k$ is calculated. For the domains in the FE model with hysteretic material properties, this is done elementwise with the provided models $\mathbf{H}^k_{\mathrm{elem}} = f(\mathbf{B}^k_{\mathrm{elem}}(t_{n+1}), \mathbf{B}_{\mathrm{elem}}(t_n))$. In case of the lamination model, (4) is solved with an inner NR loop for each element. In case of PAM, (6) can be calculated directly without any inner NR loop. For anisotropic material properties, the field components are calculated separately: $\mathbf{H}^k_x = f(B^k_x(t_{n+1}), B_x(t_n), \{p_x\})$ and $\mathbf{H}^k_y = f(B^k_y(t_{n+1}), B_y(t_n), \{p_y\})$. The updated magnetic flux density and field strength are used to update the differential reluctivity in the next NR iteration with (10), and then, (9) is solved again.

## IV. Application

The **A**-formulation with the presented material models is applied to the TEAM problem 32 that is a test case for the validation of a magnetic-field problem with vector hysteresis [13]. The hysteresis model is now parameterized by using the measured major loop of the FeSi electrical steel sheets along the rolling and transversal direction. This is supplemented by the thickness $d = 0.48\ mm$ and specific conductivity $\sigma_{\mathrm{e}} = 1.78\ (MS)/m$ to fully parameterize the lamination model. The PAM is then parameterized by means of the lamination model excited with a magnetic flux density waveform of 10 Hz and 1.5 T amplitude. The parameters of the PAM are left fixed for all excitation cases discussed in the following paragraph.

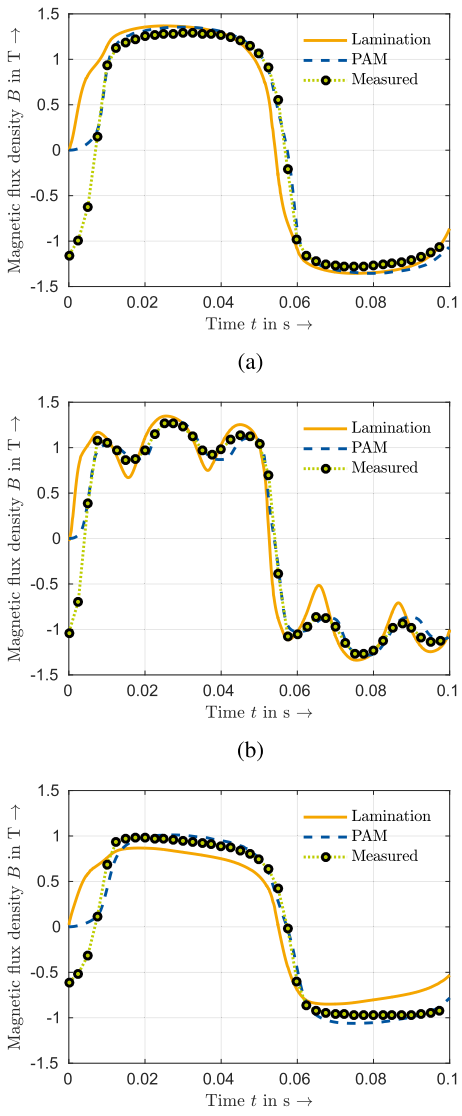


Fig. 3. Comparison of measured data (dots), theoretical predictions using PAM (dashed), and the lamination model (continuous lines) for cases 1, 2, and 4 at C6. (a) Case1. (b) Case2. (c) Case4.

Fig. 2 shows the geometry of the problem which consists of a three-limb transformer with a ferromagnetic core. On each outer limb, a winding is placed with 90 turns. Four test cases are defined for the magnetic problem: (case 1) the two windings are connected in series and supplied by a sinusoidal voltage of 13.5 V, (case 2) the same configuration is excited by the first harmonic and the fifth harmonic each with a peak value of 11.8 V, (case 3) one winding is supplied by a sinusoidal and the other by a cosinusoidal voltage both with a peak value of 14.5 V, and (case 4) one winding is supplied by a sinusoidal voltage of 10.9 V and the other is operating as the

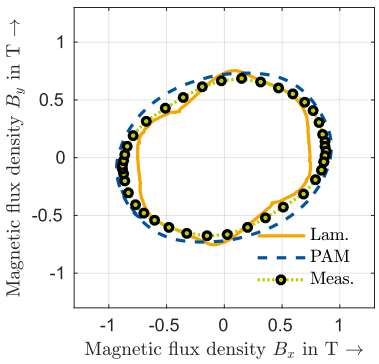


(a)

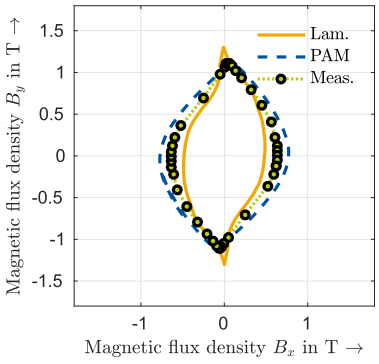


(b)

Fig. 4. Comparison of measured data (dots), theoretical predictions using PAM (dashed), and the lamination model (continuous lines) for case 3 at pick-up coils (a) C1 and C2 and (b) C3 and C4.

TABLE I
MEAN COMPUTATION TIME FOR EACH TIME STEP

| model | case 1 | case 2 | case 3 | case 4 |
|---|---|---|---|---|
| Lamination | 44.0 sec | 64.7 sec | 112.3 sec | 69.4 sec |
| PAM | 3.8 sec | 3.9 sec | 8.6 sec | 7.1 sec |

secondary winding connected to a load resistance of 0.05 Ω. The provided data in [13] for the currents in the windings serve for the source current in (9), and the measured magnetic flux densities are used for validation. The geometry is discretized by 2718 triangles with 1429 nodes. The lamination model is simulated with a time step width of 0.1 ms and the PAM with 0.5 ms.

Fig. 3 compares the measured and simulated magnetic flux density for cases 1, 2, and 4 in the central limb of the transformer (C6). It is apparent that the PAM reaches the measurement locus faster than the lamination model and that the lamination model shows a phase shift. For case 1, both models have striking accuracy. For case 2, the lamination model has higher dynamics in the fifth-order harmonic than the PAM. The PAM is almost coincident to the measured data although the parameters were identified for sinusoidal excitation on single sheets. This underlines the predictive power of the PAM. In case 4, the calculated flux density of the lamination model is lower than the results from PAM and the measurements. Excitation case 3 serves for studying the capability to describe the vectorial nature and anisotropy. Fig. 4 shows the match obtained at points C1-C2 and C3-C4. It is apparent that the PAM allows one to describe rotating fields and anisotropy, despite its simple structure. Table I shows the computation time for both models.

## V. CONCLUSION

This paper incorporates a fully coupled lamination model and an algebraic approximation (PAM) as a hysteretic constitutive law in macroscale 2-D FE simulation using the institute's in-house solver package *py*MOOSE. Both models are parameterized from standardized measurements on single sheets in rolling and transversal direction. The FE formulation and its coupling to the two models is studied by means of the 2-D simulation of a three-limb transformer (TEAM problem 32). Different excitation cases are studied covering alternating sinusoidal, non-sinusoidal, and rotating fields. Both models are compared with the measured data obtained by local pick-up coils and enable accurate simulation of the magnetic-field distribution. However, the PAM outperforms the fully coupled lamination model with $N_b = 3$ in accuracy and computational cost on a 2.9-GHz CPU core (Table I). The PAM proves to be very accurate with fixed parameters over large ranges of excitation signals, that is, one parameter set for all test cases, and allows one to account for magnetic anisotropy.

## REFERENCES

[1] S. Steentjes, F. Henrotte, C. Geuzaine, and K. Hameyer, "A dynamical energy-based hysteresis model for iron loss calculation in laminated cores," *Int. J. Numer. Model, Electron. Netw., Device, Fields*, vol. 27, no. 3, pp. 433–443, 2014.

[2] F. Henrotte, S. Steentjes, K. Hameyer, and C. Geuzaine, "Iron loss calculation in steel laminations at high frequencies," *IEEE Trans. Magn.*, vol. 50, no. 2, pp. 333–336, Feb. 2014.

[3] M. Petrun, S. Steentjes, K. Hameyer, and D. Dolinar, "1-D lamination models for calculating the magnetization dynamics in non-oriented soft magnetic steel sheets," *IEEE Trans. Magn.*, vol. 52, no. 3, Mar. 2016, Art. no. 7002904.

[4] I. Niyonzima, R. V. Sabariego, P. Dular, F. Henrotte, and C. Geuzaine, "Computational homogenization for laminated ferromagnetic cores in magnetodynamics," *IEEE Trans. Magn.*, vol. 49, no. 5, pp. 2049–2052, May 2013.

[5] F. Henrotte, S. Steentjes, K. Hameyer, and C. Geuzaine, "Pragmatic two-step homogenisation technique for ferromagnetic laminated cores," *IET Sci., Meas. Technol.*, vol. 9, no. 2, pp. 152–159, 2015.

[6] Y. Shindo, T. Miyazaki, and T. Matsuo, "Cauer circuit representation of the homogenized eddy-current field based on the Legendre expansion for a magnetic sheet," *IEEE Trans. Magn.*, vol. 52, no. 3, Mar. 2016, Art. no. 6300504.

[7] O. Bottauscio, A. Manzin, A. Canova, M. Chiampi, G. Gruosso, and M. Repetto, "Field and circuit approaches for diffusion phenomena in magnetic cores," *IEEE Trans. Magn.*, vol. 40, no. 2, pp. 1322–1325, Mar. 2004.

[8] O. Bottauscio, M. Chiampi, and D. Chiarabaglio, "Advanced model of laminated magnetic cores for two-dimensional field analysis," *IEEE Trans. Magn.*, vol. 36, no. 3, pp. 561–573, May 2000.

[9] J. Gyselinck, R. V. Sabariego, and P. Dular, "A nonlinear time-domain homogenization technique for laminated iron cores in three-dimensional finite-element models," *IEEE Trans. Magn.*, vol. 42, no. 4, pp. 763–766, Apr. 2006.

[10] P. Rasilo, E. Dlala, K. Fonteyn, J. Pippuri, A. Belahcen, and A. Arkkio, "Model of laminated ferromagnetic cores for loss prediction in electrical machines," *Electr. Power Appl.*, vol. 5, no. 7, pp. 580–588, Aug. 2011.

[11] S. Steentjes, K. Hameyer, D. Dolinar, and M. Petrun, "Iron-loss and magnetic hysteresis under arbitrary waveforms in NO electrical steel sheets: A comparative study of hysteresis models," *IEEE Trans. Ind. Electron.*, to be published.

[12] J. Gyselinck, P. Dular, N. Sadowski, J. Leite, and J. P. A. Bastos, "Incorporation of a Jiles-Atherton vector hysteresis model in 2D FE magnetic field computations: Application of the Newton–Raphson method," *COMPEL-Int. J. Comput. Math. Elect. Electron. Eng.*, vol. 23, no. 3, pp. 685–693, 2004.

[13] O. Bottauscio, M. Chiampi, C. Ragusa, L. Rege, and M. Repetto. (2002). *Description of TEAM Problem: 32 A Test-Case for Validation of Magnetic Field Analysis with Vector Hysteresis.* [Online]. Available: http://www.compumag.co.uk/